ON THE SW SEX-TYPE ECLIPSING CATACLYSMIC VARIABLE SDSS0756+0858

GAGIK TOVMASSIAN, MERCEDES STEPHANIA HERNANDEZ, DIEGO GONZÁLEZ-BUITRAGO, SERGEY ZHARIKOV, AND MARIA TERESA GARCÍA-DÍAZ

Instituto de Astronomía, Universidad Nacional Autonoma de México, Apdo. Postal 877, Ensenada, Baja California 22800, Mexico; gag@astro.unam.mx

*Received 2013 June 20; accepted 2013 December 10; published 2014 February 11

ABSTRACT

We conducted a spectroscopic and photometric study of SDSS J075653.11+085831. X-ray observations were also attempted. We determined the orbital period of this binary system to be 3.29 hr. It is a deep eclipsing system, whose spectra show mostly single-peaked, Balmer emission lines and a rather intense He II line. There is also the presence of faint (often double-peaked) He I emission lines as well as several absorption lines, Mg I being the most prominent. All of these features point toward the affiliation of this object with the growing number of SW Sex-type objects. We developed a phenomenological model of an SW Sex system to reproduce the observed photometric and spectral features.

Key words: binaries: eclipsing – binaries: spectroscopic – stars: individual (SDSS J075653.11+085831.8)

Online-only material: color figures, supplemental data

1. INTRODUCTION

Cataclysmic variables (CVs) are close, interactive binaries comprised of a white dwarf and a late-type, main sequence star. The latter fills its corresponding Roche lobe and loses matter via the Lagrangian L_1 point to the more massive, compact component. In most cases, the transferred matter forms an accretion disk around the white dwarf if the former has no strong magnetic field. The observational characteristics of CVs, upon which they are normally classified, depend greatly on the orbital period of the system, the mass accretion rate, and the strength of the above-mentioned magnetic field. The orbital period reflects not only the separation of the binary components, but also the size of the Roche lobe-filling secondary and therefore its evolutionary status. In particular, CVs with periods over \sim 3 hr still contain secondaries with radiative cores, and thus rely on magnetic breaking as a driving force to remove the angular momentum (Rappaport et al. 1983). Systems with periods below this 3 hr threshold contain red dwarfs, which are fully convective. The magnetic breaking then becomes negligible, halting the mass transfer. Before this happens, a significant number of CVs, known as SW Sex-types, are observed within the 3 \sim 4 hr period range (Schmidtobreick 2013). The SW Sex stars were first identified by Thorstensen et al. (1991) as eclipsing systems, which show characteristics very similar to each other and quite different from other CVs. Apart from wide, non-symmetric eclipses, SW Sex stars exhibit high excitation lines as well as absorption features, shifts between eclipse and emission line phasing, and single-peaked line profiles (unusual for eclipsing binaries) containing accretion disks (Dhillon et al. 1991; Hellier 2000; Hoard et al. 2003; Rodríguez-Gil et al. 2007a). They are also defined as nova-like because the highmass transfer rate helps to maintain a hot and stable accretion disk devoid of dwarf-nova-type outbursts. A detailed description and discussion of properties of SW Sex stars can be found in a number of papers from the discovery of the phenomenon (Thorstensen et al. 1991) to the latest reviews (Rodríguez-Gil et al. 2007a; Dhillon et al. 2013).

SDSS J075653.11+085831.8 (hereafter SDSS0756+0858) was identified as a CV by Szkody et al. (2011) from the SDSS DR7 lists. From a very limited time coverage (~1.5 hr) they

suggested that the object may have a period around two hours and thought it could be an intermediate polar. Since they covered slightly less than the actual orbital period of the system, they probably missed the eclipse, without which a correct identification becomes very difficult. We observed the object during two seasons in 2012 and 2013 by means of spectroscopy and multicolor photometry. We find that SDSS0756+0858 is a bonafide member of the SW Sex stars. Here, we present the results of our observations, and discuss the deduced parameters of the system and its geometry. The observations and data reduction are described in Section 2, while the results are presented and discussed in Sections 3–5. In Section 6, we present our model of SW Sex stars and draw brief conclusions in Section 7.

2. OBSERVATIONS AND DATA REDUCTION

2.1. Photometry

Time-resolved photometry of SDSS 0756+0858 was obtained using the direct CCD imaging mode of the 0.84 m telescope of the Observatorio Astronómico Nacional at San Pedro Mártir (OAN SPM)¹ in Mexico. We obtained a long series of photometry in the V band and one or two orbital periods with each UBRIJohnson-Cousins filter. The log of photometric observations is given in Table 1. The photometric data were calibrated using Landolt standard stars. The errors, ranging from 0.01 to 0.05 mag, were estimated from the magnitude dispersion of comparison stars with similar brightness. The light curve shows deep (\sim 2 mag) and wide (\sim 0.2 $P_{\rm orb}$) eclipses. Outside the eclipse, the object brightness varies smoothly with superposed shorttime flickering. The ingress to the eclipse is steeper than the egress. Such an eclipse shape is very common for SW Sex stars (Thorstensen et al. 1991) and was a defining feature of the class until it was later revealed that there are also non-eclipsing SW Sex stars (Rodríguez-Gil et al. 2007b).

In Figure 1, the V-band light curve, comprised of nine orbits and folded with the orbital period, is presented. The period determination is described in the next section. Two cycles are plotted to separate two distinct light curve morphologies. The left panel shows two orbits with a distinct hump before an

¹ http://www.astrossp.unam.mx

Table 1Log of Observations

Spectrosopy ^a Date	Coverage (hr)	Resolution FWHM (Å)	Exposure (s)
2012 Feb 1	7.3	2.1	600–1200
2012 March 4	5.8	4.4	600-1200
2012 Dec 5	1.2	2.1	900
2012 Dec 6	3.4	2.1	900
2012 Dec 7	1.5	2.1	1200
2013 Jan 16	2.6	2.1	1200
2013 Jan 17	5.4	2.1	1200
2013 Feb 6	3.1	6.5	600
2013 Feb 7	4.9	6.5	600
Photometry ^b		Filter	
2012 Feb 1	9	V	40
2012 Feb 3	2.4	B/V/R/I	60-120
2012 March 4	6.2	V	60
2012 March 5	6	V	40
2013 Jan 17	4.0	B	90
2013 Jan 19	9.8	V/R	120
2013 Jan 20	7.6	U/I	90-120
2013 Feb 6	4.4	$\stackrel{'}{V}$	120
2013 Feb 7	5.4	V	120

Notes.

eclipse, and a pronounced dip around phase $\phi \sim 0.6$ –0.7. In the right panel, the remaining light curves are combined, where the pre-eclipse hump is not so prominent and there is a distinct depression of brightness right after the eclipse. The dip around phase $\phi \sim 0.6$ is also not as defined as it is in the left panel. In both cases, the object reaches maximum brightness at phase $\phi \sim 0.4$.

2.2. Spectroscopy

We obtained long-slit spectroscopy of SDSS 0756+0858 during several observing runs using the 2.12 m telescope and the Boller & Chivens spectrograph at OAN SPM. Two different gratings were used. The 12001 mm⁻¹ grating was used to obtain the emission line profiles with the highest possible spectral resolution (up to 2.1 Å FWHM in the covered range $\sim 4000-5200$ Å) in this faint $V \sim 16.25$ object. In addition, 6.5 Å resolution spectra with a higher S/N ratio were obtained with a 400 l mm⁻¹ grating, to study the spectral energy distribution of the system, with a broader wavelength coverage (~4000–7200 Å). Observations were made with a 1".5 slit, oriented in the east-west direction. CuNeArg arcs were taken every 30-40 min for wavelength calibration. The spectrograph flexions have also been checked with the nightsky lines. Spectrophotometric standards from Oke (1990) were observed each night for flux calibration. Flux losses due to the slit width and slit orientation have not been taken into account, but in some cases we have obtained simultaneous photometry and can flux-calibrate them, if necessary. The log of spectroscopic observations and the details of the instrumental setting are provided in Table 1.

The median of all 28 spectra of SDSS 0756+0858 taken on 2013 February 7, is presented in Figure 2. The object shows single-peaked emission lines of hydrogen (Balmer series), He I lines, He II λ 4686, Bowen fluorescence C III/N III $\lambda\lambda$ 4640-4650 and C II $\lambda\lambda$ 4267, 7231, 7236 lines. Only im-

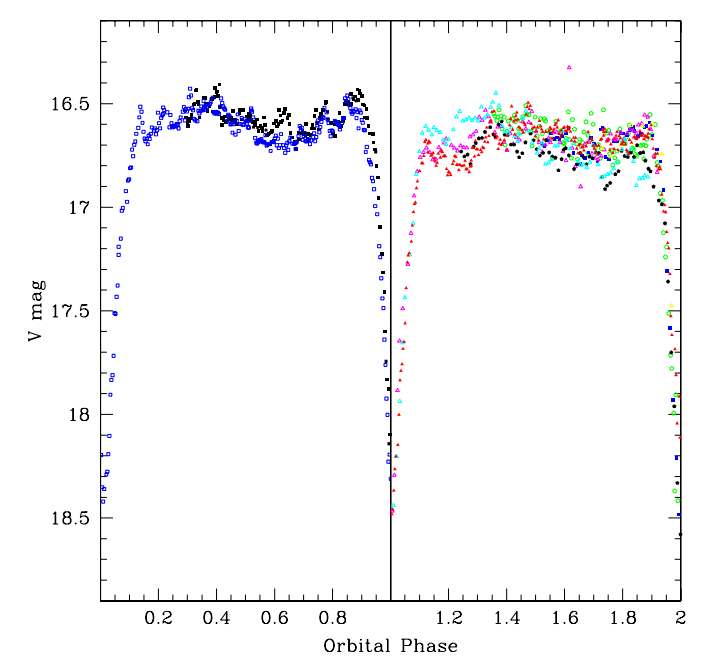


Figure 1. *V*-band light curve of SDSS 0756+0858 folded with the orbital period (see Section 3). Left panel: a few orbits of *V*-band light curves with a distinct hump before the eclipse, and a pronounced dip around phase 0.6–0.7 are presented. Right panel: the rest of the light curves without the pre-eclipse hump and with a depression after the eclipse are shown.

(A color version of this figure is available in the online journal.)

mediately before the eclipse do they show a split, which is better pronounced in the H_{α} line. He i lines show transient double peaks more often. Absorption features are also transient. The most prominent among them is the Mg line blend around $\lambda 5175$. The spectra taken in different epochs did not vary much in shape, therefore the spectrum in Figure 2 is representative of the object.

The parameters of spectral lines (radial velocities (RV), intensities, and FWHM) were measured by fitting a single Lorentzian to the emission lines, which describes observed profiles of lines much better (more completely) than a Gaussian profile. The reason is obvious: the lines are wider because they are formed in an extended area with different velocities. Often, broad emission lines of CVs are measured by the so-called double Gaussian method. This procedure is very useful when dealing with the lines formed in an accretion disk, and it allows one to measure velocity amplitude close to the central star. However, in this case, we do not think the lines are formed in the entire disk (see the interpretation of the system below), and therefore we did not implement this method. As an additional measure, we have repeated the analysis of lines by Gaussian fitting, and no substantial differences in our results were notable.

Further discussion on spectral behavior of the object is presented below in Section 5.

2.3. X-Ray Observation

The *Swift* observations of SDSS 0756+0858 in 2012 November were obtained as a target of opportunity (ObsID 00045632006), prompted by the suspicion that the object is a magnetic CV (Szkody et al. 2011). The *Swift* X-ray Telescope data were processed with standard pipeline procedures. A 10 ks long exposure showed no detectable signal from the object (≤ 0.005 counts s⁻¹).

^a 2.12 m telescope.

^b 0.84 m telescope OAN SPM.

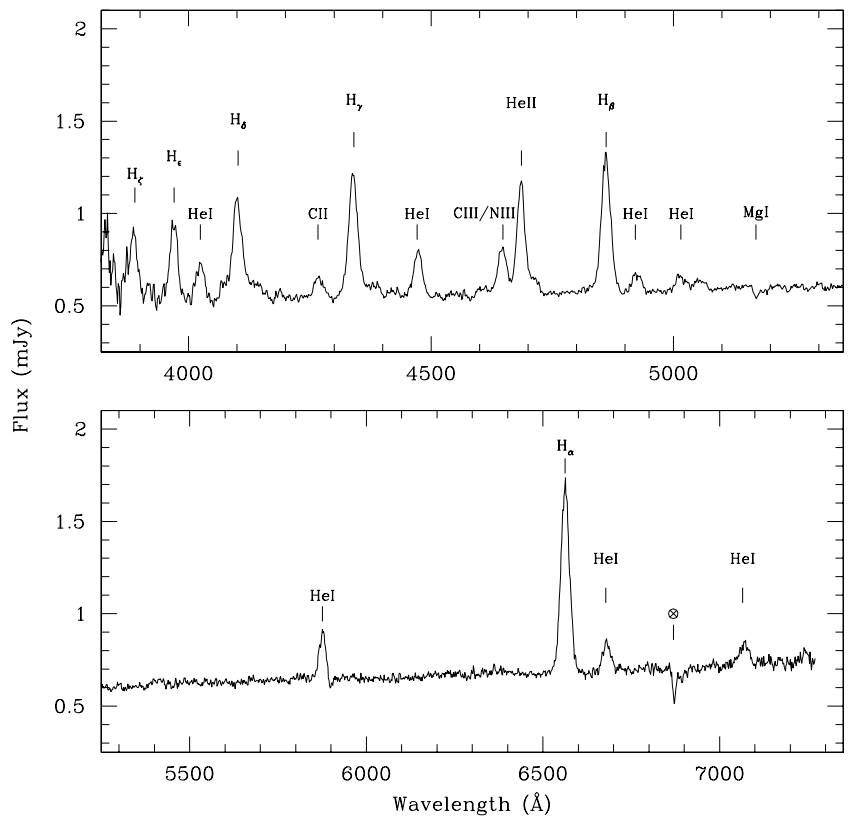


Figure 2. Average spectrum of SDSS 0756+0858. The major lines are marked.

3. THE ORBITAL PERIOD

The orbital period of SDSS 0756+0858 was determined on the basis of all acquired light curves, and (V band) and H_{β} RV variations by means of discrete Fourier transform (DFT), as implemented in $Period04.^2$ The resulting power spectra are presented in Figure 3. There appears to be one dominant frequency in the power spectra of photometric and RV data sets. As usual, they are contaminated with alias periods caused by observational cycles and frequencies of data measurement. Although the peak frequency was obvious, we analyzed the RV data for periods using CLEAN (Schwarz 1978), a DFT method, which convolves the power spectrum with the spectral window to eliminate alias frequencies originating from uneven data distribution. The peaks in the power spectra of photometric and RV data closely coincide and correspond to the orbital period of the system.

The ephemeris deduced from the period analysis is

$$HJD = 2455958.59184 + 0.1369745(4) \times E$$
,

where HJD_0 refers to the eclipse center.³ We folded all of the *V*-band data with the orbital period and obtained results consistent with the curves presented in Figure 1 (with only slight differences outside eclipse. The RV curves of H_α , H_β , and He II, folded with the orbital period, are presented in Figure 4. Two-thirds of the spectral observations were made using the higher spectral resolution mode, but there is no notable difference in RV measurements between the two sets. Least-square sinusoidal



See the reference to the program for the uncertainties estimate.

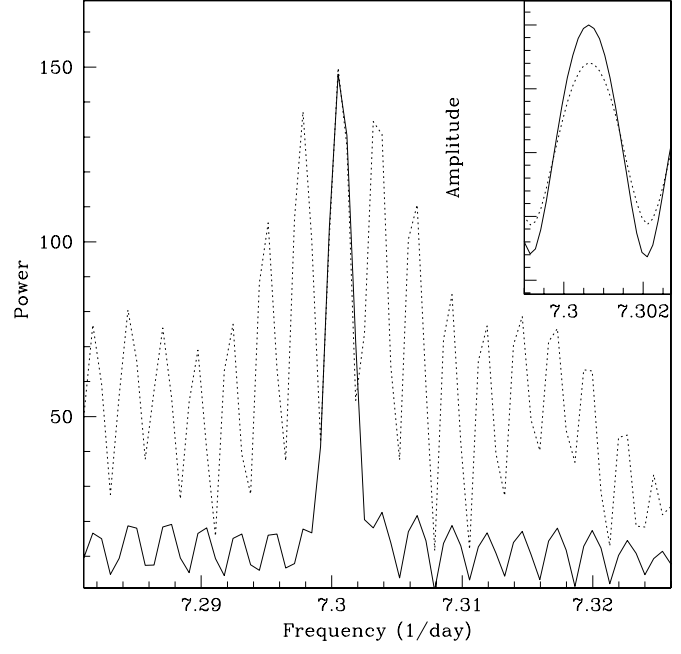


Figure 3. Power spectra of SDSS 0756+0858, obtained from DFT analysis. The dotted line is the spectrum obtained for H_{β} RVs. The solid line is the same after alias frequency cleaning. In the inset of the figure only, the highest peak is plotted (and the amplitude of the power spectrum obtained from the photometry is over-plotted). There is excellent coincidence of frequencies, but, since the amplitudes are very different, the curves were scaled to fit in the same frame.

fits to the data for each emission line were calculated in the form of

$$RV(t) = \gamma + K_{em} \times \sin(2\pi t/P + \phi),$$

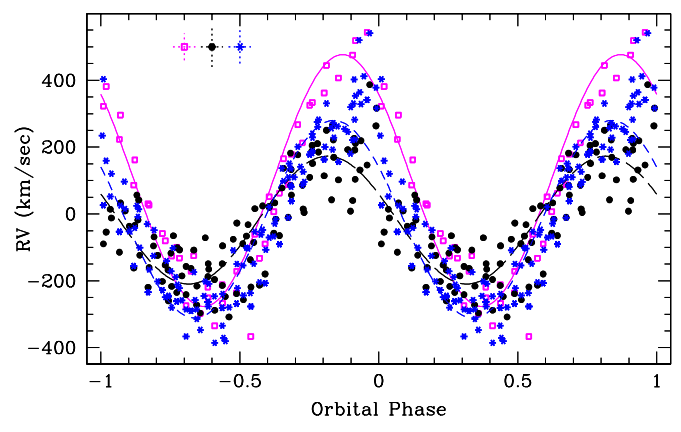


Figure 4. Radial velocity curves of SDSS 0756+0858. The solid, black circles are measurements of the He II line, and the black, long-dashed line is a sinusoidal fit to the data. The blue stars and blue, dashed line correspond to H $_{\beta}$, and the magenta, open squares and solid line are the measurements and fit for the H $_{\alpha}$ line. All three lines show the different semi-amplitudes of radial velocities and phase shifts relative to each other, as can be seen also from Table 2. Phase zero corresponds to the eclipse. Two orbital periods are repeated for better presentation.

(A color version and supplemental data of this figure are available in the online journal.)

Table 2Radial Velocity Fit Parameters

Line ID	γ (km s ⁻¹)	Velocity (km s ⁻¹)	Phase Shift ϕ^{a}
$\overline{H_{\alpha}}$	100.2	376.8	0.88
	-15.7	295.4	0.91
Н _β Не п ^b	-18.3	191.3	0.93

Notes

where γ is the systematic velocity, $K_{\rm em}$ is the semi-amplitude of RV, and ϕ is the zero-phase. The resulting values of γ , $K_{\rm em}$ and ϕ are presented in Table 2.

4. PHASE DEPENDENT PARAMETERS

The eclipse profiles of SW Sex stars are usually nonsymmetric and vary in shape with time (Thorstensen et al. 1991). In the case of SDSS 0756+0858 the profile has stayed fairly stable over the course of our two-year monitoring. The light curve, outside the eclipse, is relatively flat. There is a small hump that appears immediately before the eclipse and a depression appears after it, as the system emerges from it (see Figure 1). The brightness then increases, peaking around $\phi = 0.4$, and experiences another depression around $\phi = 0.6-0.7$. This behavior is seen, generally, in all other eclipsing SW Sex stars (Thorstensen et al. 1991; Hoard et al. 1998). In addition to the long series of V photometry, we obtained multi-color UBVRI light curves of subsequent orbital cycles (see Figure 5, left). Apparently, the pre-eclipse hump is more prominent in the blue end of the optical spectrum (B & V bands), while it is almost nonexistent in the I band. At the same time, the eclipse depth decreases to the red. We can assume that, in eclipse, a hot source of continuum light is getting blocked by the secondary star, while the disk is not eclipsed entirely, and some cooler parts contributing to R and I bands are always visible. More telling are the variations of the emission line parameters presented on the right side of Figure 5. In the upper panel, the intensity

variation of H_{α} , H_{β} , and $He\,\textsc{ii}$ lines are presented. The depth of eclipse increases with the excitation level of the line, H_{α} is a little obscured; its flux drops almost as much as in the counter-eclipse phase. H_{β} is probably produced in a more compact area and its eclipses are deeper. The high excitation line $He\,\textsc{ii}$ declines the most. The semi-amplitude of the $He\,\textsc{ii}$ RV is also significantly smaller than that of the Balmer lines (Figure 4). The orbital variability of the emission line full widths (FWHM) is shown in the right, lower panel in Figure 5. Here, $He\,\textsc{ii}$ is almost flat for most orbital phases, while the Balmer lines vary greatly; the lower excitation line becoming much broader, both around the eclipse and half the orbital phase.

The behavior of H_{α} , H_{β} , He II, He I, fluorescent emission lines C III/N III, and the Mg I absorption, is depicted in a different manner by the trailed spectra in Figure 6. The trailed spectra were formed using relatively high S/N spectra, obtained on two consecutive nights in 2013 February. Among the features that are notable in the trailed spectra are:

- 1. Right before the eclipse (starting from $\phi = 0.8$) there is a sharp zigzag in the emission lines.
- 2. At phase $\phi = 0$ (eclipse) there is a "tail" in emission extending to velocities exceeding 2000 km s⁻¹.
- Balmer lines are narrower and appear more intense at phases φ = 0.25 and 0.75 as demonstrated in the lower right panel of Figure 5.
- 4. Around phases $\phi = 0.4$ –0.6 emission lines become broader, some He I lines become double-peaked. There is flaring of lines at these phases, a feature common to SW Sex objects.

Another common feature of SW Sex stars is the appearance in their spectra of absorption lines not associated with the secondary. We can see that the Mg I "b" line appears in almost all phases, but becomes more visible around phase $\phi=0.45\pm0.2$. This is also the phase when the emission lines become broader, probably due to a high velocity component and flaring. The He I line practically splits at that phase.

5. DISCUSSION

This new CV, discovered by the SDSS, exhibits all of the attributes necessary for it to be classified as a SW Sex star. It has a 3.29 hr orbital period, placing it in the middle of the SW Sex stars' period distribution, next to DW UMa, a classic representative of the class with which it shares many common features, as outlined by Araujo-Betancor et al. (2003); Dhillon et al. (2013). Two other similar systems, 2MASS J01074282+4845188 and HBHA 4705-03, have recently been discovered (Khruzina et al. 2013; Yakin et al. 2013, although the latter is not recognized as an SW Sex star), and are not yet included in the big-list of SW Sex objects compiled by Hoard.⁴ But the number of CVs in the \sim 3–4 hr orbital range bearing characteristics of SW Sex stars grows, and curiously, the fraction of eclipsing systems among SW Sex-type grows too, although we are far from understanding the phenomenon itself. Besides the V-shaped and non-symmetric eclipses, SDSS 0756+0858 shows high velocity and single-peaked emission lines forming a characteristic "S-wave" with phase shifts between different lines (Figure 4). Even the lowest measured RV amplitude encountered in He II $(\sim 200 \text{ km s}^{-1})$ is too high to be ascribed to the orbital velocity of a white dwarf in a CV with a three-and-a-half-hour orbital period. Such systems would normally consist of a $0.6-0.7M_{\odot}$

^a P_{orb} and HJD₀ determined from the eclipse ephemeris.

^b λ4686

⁴ http://www.dwhoard.com/biglist

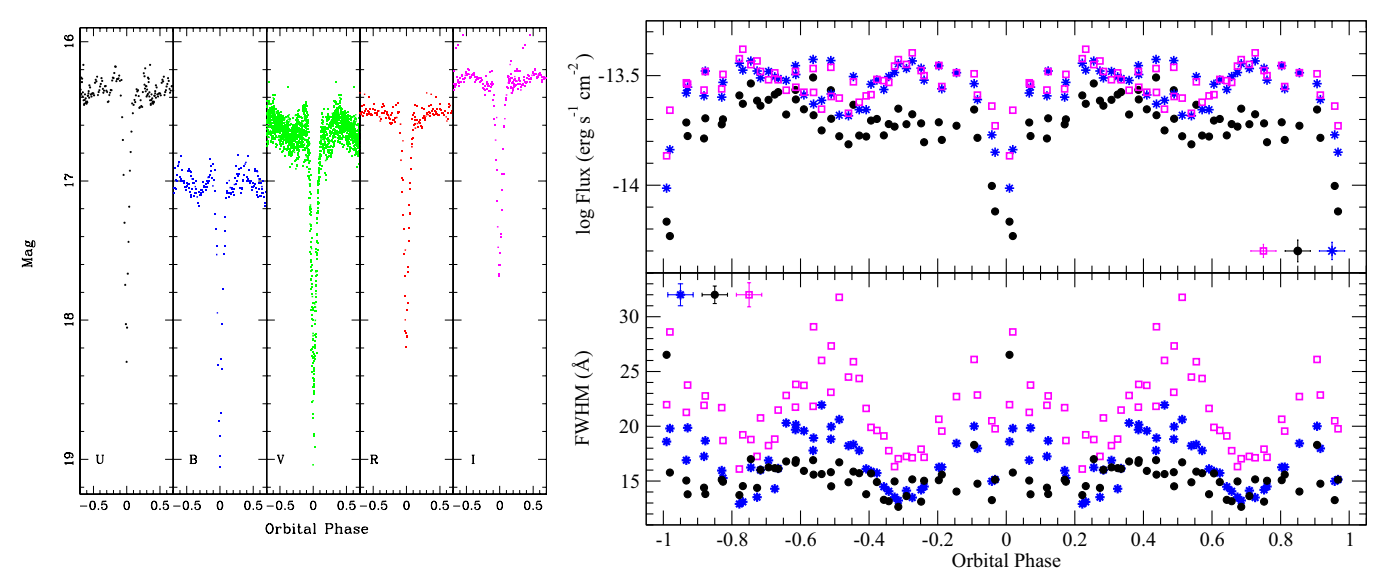


Figure 5. UBVRI light curves of SDSS 0756+0858 (left). Line parameters of SDSS 0756+0858 (right). In the upper panel, the fluxes of He II (black), H $_{\beta}$ (blue), and H $_{\alpha}$ (magenta) emission lines are plotted vs. orbital phase. In the lower panel, FWHM measurements of same lines are presented. The Balmer lines show a much larger broadening around phase 0.5 than He II. At the same time, He II shows deeper eclipses than the lower excitation lines. For the sake of clarity, the data are repeated in the right panel to cover two orbital periods.

(A color version and supplemental data of this figure are available in the online journal.)

white dwarf and a $0.25 \pm 0.05~M_{\odot}$ secondary, with maximum RV semi-amplitudes for the white dwarf and the secondary star reaching $\sim \! 100$ and $\sim \! 300~{\rm km~s^{-1}}$, respectively. Otherwise, the system should contain either an abnormally light-weighted white dwarf, or an unrealistically massive secondary star.

The single-peaked emission lines remain the most baffling features of SW Sex stars. Most authors employ models that help to elevate the ionized matter above the orbital plane to explain the formation of such line profiles, i.e., bright-spot overflow plus accretion disk wind (Honeycutt et al. 1986; Hoare 1994; Dhillon & Rutten 1995), magnetic accretion column (Williams 1989), or magnetically driven outflow (Tout et al. 1993; Wynn & King 1995). These may not be necessary, if we take a clue from the study of BT Mon, an old nova with a full range of SW Sex observational characteristics, by White et al. (1996). These authors show that the emission lines originate where the bright spot should be (or slightly further), yet they claim that they do not see the presence of an accretion disk. Let us keep in mind that SW Sex stars are high mass transfer rate systems and they have steady hot disks similar to those of dwarf novae in outburst (Szkody et al. 1990). Such disks are optically thick and maintain a delicate balance of absorption and emission lines, often appearing almost featureless. We may assume, that in SDSS 0756+0858 and other SW Sex objects, the accretion disk has a large contribution in the continuum but little in the lines and that the bright spot is either the only or the dominant source of the emission lines. Thus, the observer of spectral lines "does not see" the presence of the accretion disk and detects only single-peaked emission lines from an area known as the bright spot. This can be exacerbated by the elongated, down stream bright spot and the geometrical thickness of disk edges, shadowing the emission from its surface.

In fact, Dhillon et al. (1997) proposed the exact same idea; they even considered an extended bright spot. But they stopped short of affirming the presence of such structure in the disk citing an absence of detailed hydrodynamical calculations describing it. Recently, Bisikalo et al. (2008) and Kononov et al. (2012) performed such three-dimensional gas-dynamical simulations

for accretion disks. Their calculations show the flow of matter in SS Cyg, a dwarf nova with a $\dot{M} \sim 8 \times 10^{-9} M_{\odot} \text{ yr}^{-1}$ mass transfer rate, a typical value for a dwarf nova. One would expect that the effects obtained in that simulation would become more important with an increase in the mass transfer rate. According to their calculations, apart from the stream of matter from the secondary star feeding the accretion disk , there is an outflow of matter leaving the accretion disk and forming a circum-disk halo. The former apparently plays an important role in SW Sex stars as it does in all interacting binaries. In this case, its role is enhanced by the extension of the spot into what (Bisikalo et al. 2008) call a "hot line," or arc. Consideration of the latter, i.e., the outflow of matter from the disk, can help to explain the additional features. We can see, in the right panel of Figure 5, that in phase $\phi = 0.5$, the Balmer lines are twice as broad as they are in other phases, but their intensity decreases. They also show irregular variations in width, also called line flaring. This can be explained by the presence of the circum-disk halo which produces lines with broader velocities. It can also be responsible for the appearance of the absorption features. At $\phi = 0.25$ and $\phi = 0.75$, both streams are viewed perpendicular, thus the dispersion of the velocities is smaller and the lines narrower. During the eclipse, the halo remains mostly visible, preventing a total eclipse of the low-excitation lines. The system brightens at $\phi = 0.3$ –0.4 and exhibits irregular variability, which Dhillon et al. (2013) explain as a non-uniform disk edge. Their model does not explain why it is non-uniform, or why the rim on that side of the disk is not as wide. Knigge et al. (2004) came to a similar conclusion using UV spectra, noting a presence of absorbing material at the phase opposing the eclipse and its non-uniform physical conditions. However, if there is outflow, then it will probably introduce a necessary non-uniformity to the disk edge. The flaring of the emission lines has been interpreted as evidence of magnetic accretion (Rodríguez-Gil et al. 2001; Rodríguez-Gil & Martínez-Pais 2002; Rodríguez-Gil et al. 2009). This claim is supported by evidence of the periodic nature of flaring, and in some cases, a more substantial indication is the detection

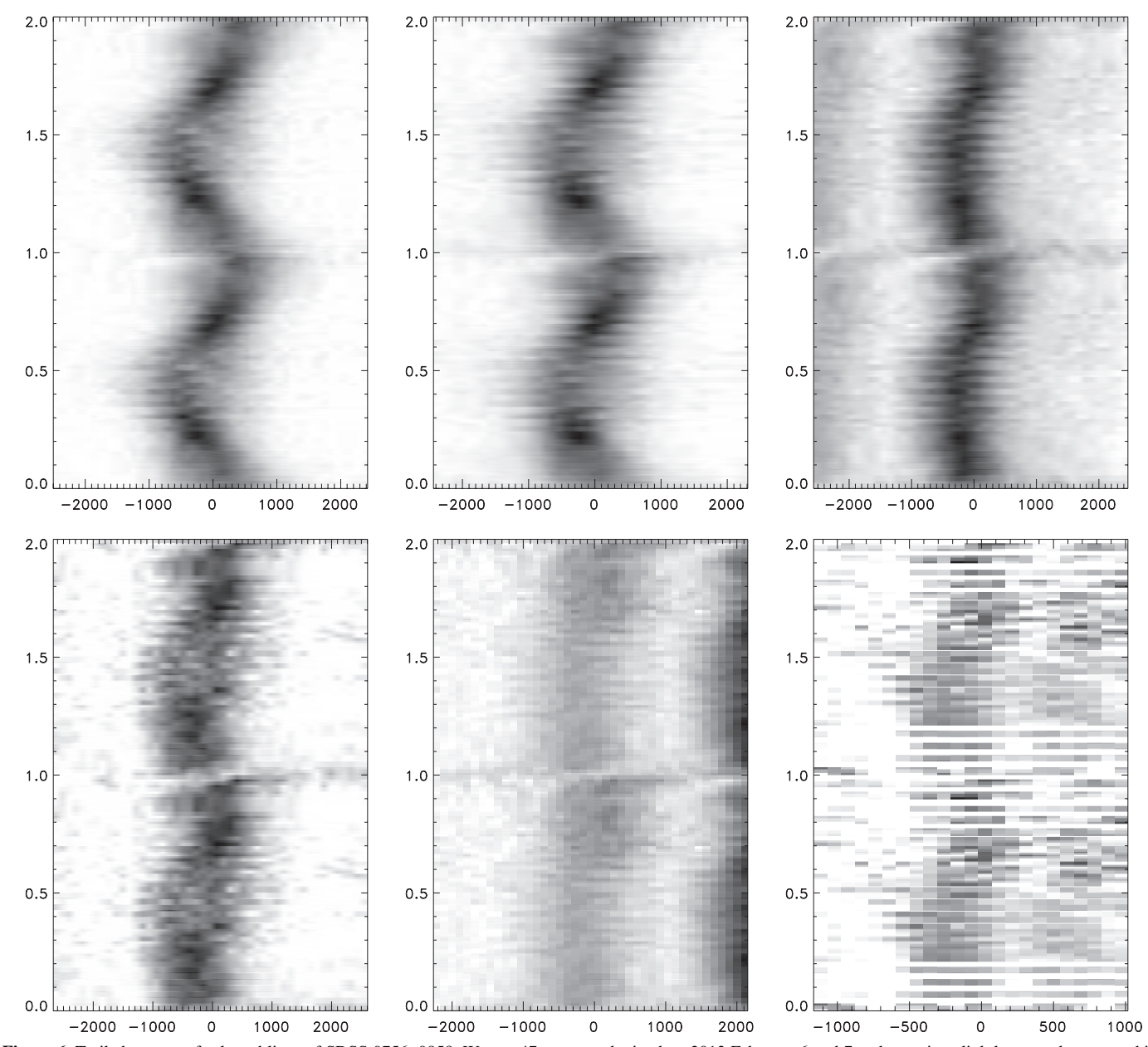


Figure 6. Trailed spectra of selected lines of SDSS 0756+0858. We use 47 spectra, obtained on 2013 February 6 and 7 and covering slightly more than two orbital periods to construct the images. From the top left to the right, in separate panels, H_{α} , H_{β} , and $He\,\textsc{II}$ are presented, and at the bottom, also from the left to right: $He\,\textsc{I}$ λ 4471, complex of fluorescent lines $C\,\textsc{III}/N\,\textsc{III}$, and $Mg\,\textsc{I}$ (inverse gray scale, since the line is in absorption).

of circular polarization. We do not question the presence of magnetic white dwarfs in SW Sex stars or truncation of the accretion disk, but we do not have any magnetic manifestation in the case of SDSS 0756+0858. We analyzed the equivalent width variability of H_{β} and He II lines and found no periods except the orbital period, and an alias related to the exposure length of individual spectra. We also believe that magnetic accretion, modulating the emission line width, would produce substantial X-ray emission, but we detected none.

6. THE MODEL

We developed a geometric model of an SW Sex system, presented in Figure 7, to reproduce the observed photometric and spectral features of SDSS 0756+0858. The system is comprised of a primary white dwarf, a secondary red dwarf star, a stream of accretion matter, a thick $z^d(r) = z^d(r_{out})(r/r_{out})^v$ accretion

disk, and an elongated and extended hot spot/line. The white dwarf is a sphere, defined by the mass–radii relation in Warner (1995, 2.83b). The secondary is assumed to fill its Roche lobe, and the Roche lobe shape is directly calculated using Equation (2.2) (Warner 1995) for equipotential $\Phi(L_1)$. The mass and temperature of the primary are defined as initial parameters. The mass of the secondary is obtained from the mass–period relation 2.100 (Warner 1995), which also defines the effective temperature of the secondary, using relations $\log T_2^{\rm eff} \propto \log M_2$ from Malkov (2007). The illumination of the secondary by the primary is also included. A standard temperature gradient

$$T^d(r) \sim T_* \times r^{-3/4}$$
,

where

$$T_* = \left(\frac{3GM_{\rm wd}\dot{M}}{8\pi\sigma R_{\rm wd}^3}\right)^{1/4}$$

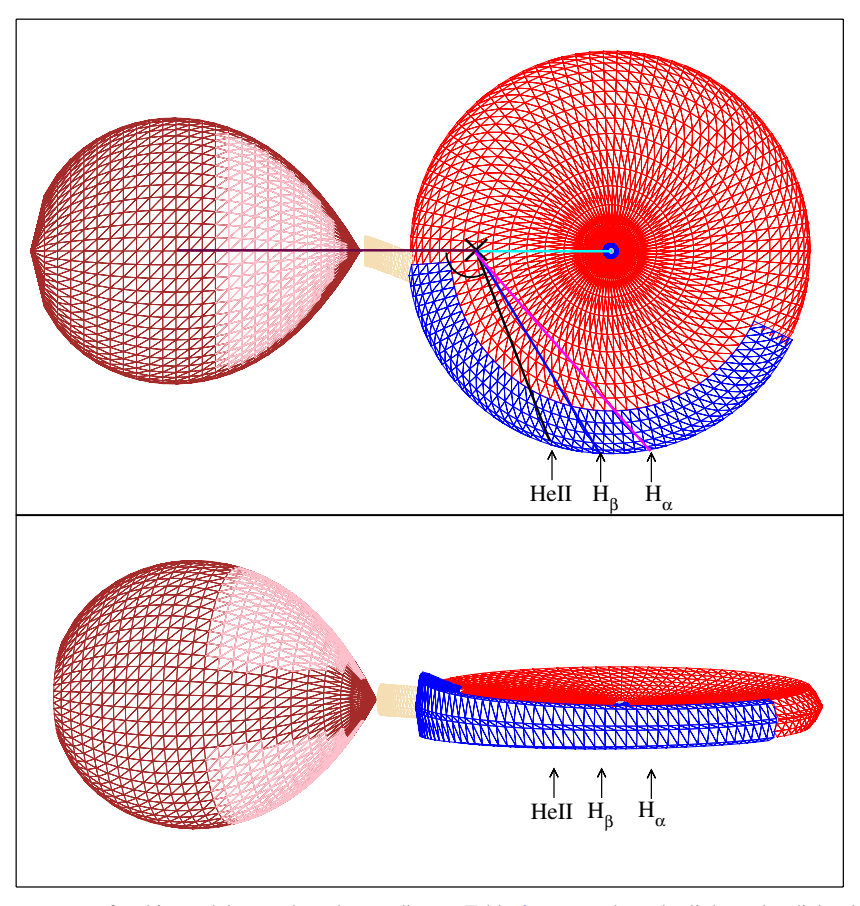


Figure 7. SW Sex model. The parameters for this model are selected according to Table 3 to reproduce the light and radial velocity curves closely resembling the observations. The calculated curves are presented. The extended hot spot, or hot line, is drawn in blue. Marked are the weighted centers of areas where the corresponding emission lines are formed. Because of the temperature gradient in the arc and stratification of lines, each of them revolves around the center of mass, denoted by "x," with different velocity and phase.

(A color version of this figure is available in the online journal.)

(see 2.35, 2.36, 2.37 Warner 1995) between the inner and the outer edges ($r_{\rm out} \approx 0.60a/(1+q)$) of the disk was assumed. The impact of the stream with the outer rim of the disk forms a shock-heated trailing arc along the rim as was described by the schematic model of Hoard et al. (2003, Figure 12 therein) and the hotline defined in Bisikalo et al. (2008). The vertical size z_s and the temperature T^s of the arc-like hot spot are not uniform; it is wider and hotter at the impact point ($\varphi_{\rm min}$) and declines both in temperature and vertical extension, according to an arbitrarily selected manner described in the following equations:

$$T^{s}(\varphi) = T^{d}\left(1.0 + \gamma^{T} f(\varphi)^{\frac{3}{2}}\right)$$

$$z^{s}(\varphi) = z^{d} \left(1.0 + \gamma^{z} f(\varphi)^{\frac{5}{2}} \right),$$

where φ is the angle between the line connecting the stars in conjunction and the direction of the spot viewed from the center of mass; $f(\varphi) \equiv a \times \varphi + b$ is a linear function with constants a and b, defined by the boundary conditions of $f(\varphi_{\min}) = 1$, and $f(\varphi_{\max}) = 0$, and γ^T , γ^z are free parameters.

The surface of each component of the system is divided in a series of triangles, as shown in Figure 7. We assume that each triangle emits as a blackbody with corresponding temperature. Figure 8 presents geometry snapshots (top) and the model calculations of light and RV curves (bottom two). The light curves of individual components of the binary system were obtained

by integrating the emission from all the elements lying in view, and are presented in the middle panel of Figure 8. The flux from the white dwarf is almost totally blocked by the thick disk. Two equally dominant sources of emission from the model light curves are the accretion disk and the bright spot/arc (denoted by the red and blue lines, respectively). The disk's contribution is more significant after the eclipse, when the bright spot is largely hidden behind it. In contrast, the form of the light curve before the eclipses is mostly determined by the bright spot. The eclipse corresponds to the blockage of the bright spot by the secondary. Thus, the observational phase, $\phi = 0$, which is assigned to the conjunction of the stellar components, does not coincide with the zero phase in Figure 8. The fit is not optimized mathematically, but it is sufficient to explain all the observed features: the eclipse, the pre-eclipse-hump, the depression around phase 0.6–0.7, and even the little wiggle at $\phi = 0.18$ reasonably well. The main parameters of the model are given in Table 3. We can achieve a satisfactory qualitative resemblance between the modeled light curves and the observations by simply varying the system inclination and the hot spot parameters. All other parameters are fixed.

The model also effectively describes the amplitude and phase of the emission lines as basically emanating from the hot spot. Since the hot spot is extended, and its temperature is the highest at the impact point, there is a stratification of temperatures, and hence the excitation levels along the arc. The lines of different excitation energies are predominantly formed at a

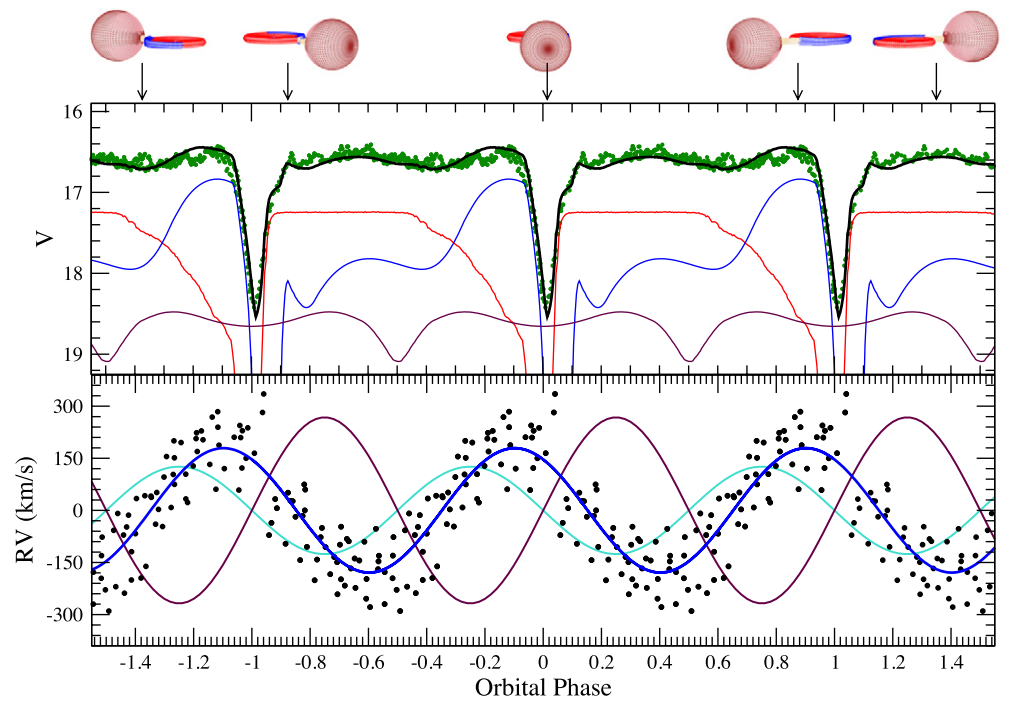


Figure 8. Light and radial velocity curves calculated from the model. At the top of the figure, five different perspectives of the model are presented. Their corresponding phases are marked by ticks on the outer side of the upper panel. Phase 0.0 in this figure corresponds to the inferior conjunction, unlike previous figures where it corresponded to the eclipse center ($\phi = 0.025$ difference). In the upper panel, the computed V-band light curves of the disk (red), the hot spot (blue), and the secondary star (brown) are plotted along the sum of all components, presented as a black line. The green points are observations in the V-band. The contribution of the white dwarf is negligible and lies outside of the figure. In the bottom panel, the computed radial velocities of stellar components are presented. The higher velocity brown curve corresponds to the secondary star and the cyan to the white dwarf. They are not observed. The points correspond to the observed radial velocity of the He II line, and the blue curve is the computed velocity from the model. Two Balmer lines marked in Figure 7 are not presented, so as not to complicate the plot, but they describe the observed points as adequately as the He II.

(A color version of this figure is available in the online journal.)

Table 3
Parameters Used to Compute the Photometry and Radial Velocity Curves from the Model

System input:		
Period	11834.6 s	
Mass of primary	$0.6~M_{\odot}$	
Mass ratio	0.47	
System inclination	84°	
Radial disk size r_{out}	$0.40~R_{\odot}$	
Vertical disk size $z^d(r_{out})$	$0.10~R_{\odot}$	
v radial slope	3	
\dot{M}	$1.2 \times 10^{-10} M_{\odot} \mathrm{yr}^{-1}$	
Distance	290 pc	
Hot spot/line:		
Width	$0.2 \times r_{\text{out}}$	
Length	140°	
γ^T	0.75	
γ^z	0.75	
System output:		
Mass of secondary	$0.28~M_{\odot}$	
T_2	3250 K	
a separation	$1.07~R_{\odot}$	

different angles from the mass center, as marked in Figure 7. He II arises from an area located closest to the binary's center of mass, and thus, has the lowest amplitude of RV. The lower the excitation level, the further the weighted center of the line of

the forming region is along the arc, and, therefore, the larger the RV amplitude is. The phasing of the lines, relative to the orbital phase, changes accordingly. In the bottom panel of Figure 8 the calculated RV curve of the He II line is presented, and it excellently describes the points obtained from the observations. Also shown are calculated velocities of stellar components, which are not observed. Calculated velocities of Balmer lines are not presented, so as not to crowd the figure.

The model is also able to describe fine details, in particular, what happens in phases $\phi = 0.9$ –1.0. The white dwarf (and the accretion disk in general) has already reached the maximum positive velocity, and it is moving toward stellar conjunction with decreasing RV (light blue curve). But emission lines, formed predominantly in the bright arc, still have an increasing RV, peaking around phase $\phi = 0.9$ (blue curve). Around that phase, however, the secondary starts eclipsing part of the bright arc where the matter with the growing velocities is concentrated, and the observer sees only the far extreme of the arc, which moves in the opposite direction. Thus, for a brief moment before the total eclipse of the bright arc, we detect a less intense emission line with decreasing RV. This creates a zigzag in the trailed spectra (see Figure 6). The zigzag is best pronounced in the He II line, since it is formed closer to the stream/diskimpact point, which is eclipsed first, leaving the rest of the arc visible. At the depth of the eclipse ($\phi = 0.025$ in phases determined by radial velocities), the very tip of the retreating half of the disk, or the hot arc, is still visible (see the cartoon at the top of the Figure 8. It contains matter moving away from the observer with the sum of Keplerian and orbital velocities, and appears in the RV curves and trailed spectra as a high velocity tail. This model does not take into account the matter outflowing from the opposite side of the hot arc side in the disk. We think that the inclusion of that element would allow fine tuning of the model to the observations.

7. CONCLUSIONS

We have unveiled a new eclipsing SW Sex star. It has an orbital period of 3.287 hr, at the center of a range of periods where the great majority of SW Sex stars cluster. It has all observational characteristics of this type of star and, as such, increases the number of eclipsing systems of this particular type at these periods. We believe that this clustering is something not well understood and should be addressed, but it is beyond the scope of this study. On the other hand, we have been able to reproduce the photometric and RV curves of SDSS 0756+0858 by simply assuming that the emission lines are predominantly formed/ observed from the hot, extended spot, without the additional speculative mechanisms proposed in other models. We think that the absence of lines from other parts of the disk is a consequence of the disk having a high temperature and surface density regime, and is partially due to self-obscuration caused by the thick rim at the same time. We also believe that there is an outflow of matter from the opposite to the arc side of the disk, where the absorption features observed in SW Sex objects are formed. That outflowing matter may also contribute to the high velocity components of the low-excitation lines.

M.S.H. and D.G.B. are grateful to CONACyT for grants allowing their post-graduate studies. G.T. and S.Z. acknowledge PAPIIT grants IN-109209/IN-103912 and CONACyT grants 34521-E, 151858 for resources provided toward this research. We would like to thank the *Swift* team for the opportunity to observe the object and their prompt response to our application. We also thank Dr. J. Echevarria for reading the article and for his critical and helpful comments.

REFERENCES

```
Araujo-Betancor, S., Knigge, C., Long, K. S., et al. 2003, ApJ, 583, 437
Bisikalo, D. V., Kononov, D. A., Kaigorodov, P. V., Zhilkin, A. G., & Boyarchuk,
   A. A. 2008, ARep, 52, 318
Dhillon, V. S., Marsh, T. R., & Jones, D. H. P. 1991, MNRAS, 252, 342
Dhillon, V. S., Marsh, T. R., & Jones, D. H. P. 1997, MNRAS, 291, 694
Dhillon, V. S., & Rutten, R. G. M. 1995, MNRAS, 277, 777
Dhillon, V. S., Smith, D. A., & Marsh, T. R. 2013, MNRAS, 428, 3559
Hellier, C. 2000, NewAR, 44, 131
Hoard, D. W., Szkody, P., Froning, C. S., Long, K. S., & Knigge, C. 2003, AJ,
   126, 2473
Hoard, D. W., Szkody, P., Still, M. D., Smith, R. C., & Buckley, D. A. H.
  1998, MNRAS, 294, 689
Hoare, M. G. 1994, MNRAS, 267, 153
Honeycutt, R. K., Schlegel, E. M., & Kaitchuck, R. H. 1986, ApJ, 302, 388
Khruzina, T., Dimitrov, D., & Kjurkchieva, D. 2013, A&A, 551, A125
Knigge, C., Araujo-Betancor, S., Gänsicke, B. T., et al. 2004, ApJL,
  615, L129
Kononov, D. A., Giovannelli, F., Bruni, I., & Bisikalo, D. V. 2012, A&A,
  538, A94
Malkov, O. Y. 2007, MNRAS, 382, 1073
Oke, J. B. 1990, AJ, 99, 1621
Rappaport, S., Verbunt, F., & Joss, P. C. 1983, ApJ, 275, 713
Rodríguez-Gil, P., Casares, J., Martínez-Pais, I. G., Hakala, P., & Steeghs, D.
  2001, ApJL, 548, L49
Rodríguez-Gil, P., Gänsicke, B. T., Hagen, H.-J., et al. 2007a, MNRAS,
  377, 1747
Rodríguez-Gil, P., & Martínez-Pais, I. G. 2002, MNRAS, 337, 209
Rodríguez-Gil, P., Martínez-Pais, I. G., & de la Cruz Rodríguez, J.
   2009, MNRAS, 395, 973
Rodríguez-Gil, P., Schmidtobreick, L., & Gänsicke, B. T. 2007b, MNRAS,
  374, 1359
Schmidtobreick, L. 2013, CEAB, 37, 361
Schwarz, U. J. 1978, A&A, 65, 345
Szkody, P., Anderson, S. F., Brooks, K., et al. 2011, AJ, 142, 181
Szkody, P., Piche, F., & Feinswog, L. 1990, ApJS, 73, 441
Thorstensen, J. R., Ringwald, F. A., Wade, R. A., Schmidt, G. D., & Norsworthy,
  J. E. 1991, AJ, 102, 272
Tout, C. A., Pringle, J. E., & La Dous, C. 1993, MNRAS, 265, L5
Warner, B. 1995, CAS, 28
White, J. C., II, Schlegel, E. M., & Honeycutt, R. K. 1996, ApJ, 456, 777
Williams, R. E. 1989, AJ, 97, 175
Wynn, G. A., & King, A. R. 1995, MNRAS, 275, 9
Yakin, D. G., Suleimanov, V. F., Vlasyuk, V. V., & Spiridonova, O. I. 2013,
   AstL, 39, 38
```